Simulations of Molecular Diffusion in Lattices of Cells: Insights for NMR of Red Blood Cells

David G. Regan and Philip W. Kuchel
School of Molecular and Microbial Biosciences, University of Sydney, New South Wales 2006, Australia

ABSTRACT The pulsed field-gradient spin-echo (PGSE) nuclear magnetic resonance (NMR) experiment, conducted on a suspension of red blood cells (RBC) in a strong magnetic field yields a *q*-space plot consisting of a series of maxima and minima. This is mathematically analogous to a classical optical diffraction pattern. The method provides a noninvasive and novel means of characterizing cell suspensions that is sensitive to changes in cell shape and packing density. The positions of the features in a *q*-space plot characterize the rate of exchange across the membrane, cell dimensions, and packing density. A diffusion tensor, containing information regarding the diffusion anisotropy of the system, can also be derived from the PGSE NMR data. In this study, we carried out Monte Carlo simulations of diffusion in suspensions of "virtual" cells that had either biconcave disc (as in RBC) or oblate spheroid geometry. The simulations were performed in a PGSE NMR context thus enabling predictions of *q*-space and diffusion tensor data. The simulated data were compared with those from real PGSE NMR diffusion experiments on RBC suspensions that had a range of hematocrit values. Methods that facilitate the processing of *q*-space data were also developed.

INTRODUCTION

Pulsed magnetic field-gradients can be used in nuclear magnetic resonance (NMR) experiments to encode spatial information in spin-magnetization to measure positional displacement. The analogy of the resulting spatial coherences seen in NMR data to optical diffraction was first pointed out by Mansfield and Grannell (1973). Cory and Garroway (1990) showed that pulsed field-gradient spin-echo (PGSE) NMR diffusion measurements in heterogeneous systems can be used to obtain a displacement profile of molecules in a liquid, allowing the delineation of features of compartments too small to be observed using conventional NMR imaging. Callaghan et al. (1991) demonstrated interference-like effects in PGSE NMR diffusion studies of fluids in porous media and recently reviewed the spatial coherence phenomena arising from these experiments (Callaghan et al., 1999). We have conducted PGSE NMR diffusion studies of red blood cell (RBC) suspensions and showed that diffusion–diffraction and diffusion–interference of water occurs; this was used to show the alignment of RBC in the static magnetic field of the spectrometer and to estimate cell dimensions, detect shape changes with time, and to estimate membrane transport characteristics (Kuchel et al., 1997, 2000; Torres et al., 1998, 1999). It has been independently demonstrated that RBC align in a strong magnetic field with their disc planes parallel to the magnetic field (Higashi et al., 1993) so this was important in the design of the diffusion-simulation models used herein (see Materials and Methods).

Diffraction-like effects from PGSE NMR diffusion experiments can be visualized by plotting the relative signal intensities as a function of the spatial wave vector $\mathbf{q}$, where $\mathbf{q} = (2\pi)^{-1}\gamma\mathbf{g}\delta$, and where γ is the magnetogyric ratio of the observed nucleus, $\mathbf{g}$ is the magnetic field gradient, and δ is the duration of each of the magnetic field-gradient pulses used in the experiment. The resulting graph (*q*-space plot), from an RBC suspension consists of a series of maxima and minima whose positions in *q* space can be related to average cell dimensions and the average spacing of the extracellular cavities or "pores" (Torres et al., 1998, 1999). The positions of these features may also change when there is a change in the rate of exchange of diffusant across the cell membrane (Kuchel et al., 1997).

We have previously used simulations of diffusion in an RBC suspension, in the PGSE NMR context, to aid in the assignment of *q*-space features to particular modes of diffusion (Torres et al., 1999). Here we extend this work and demonstrate that these simulations provide further insights that are useful for the interpretation of *q*-space and diffusion tensor data from RBC suspensions. Specifically, we show that the *q*-space and diffusion tensor data contain information relating to the packing density of the cells in a suspension and the mean cell geometry. This study, therefore, extends the methodology and concepts used in interpreting data from PGSE NMR diffusion experiments on RBC suspensions and potentially in analogous cellular systems.

MATERIALS AND METHODS

Simulations

Individual computer models were developed to simulate diffusion in a suspension of biconcave discs (Program I), and to simulate diffusion in a suspension of oblate spheroids (Program II). (All programs described in this report may be obtained from DGR at d.regan@mmb.usyd.edu.au.) These models enable the simulation of diffusion during a standard PGSE

Submitted January 21, 2002 and accepted for publication March 7, 2002.

Address reprint requests to Philip W. Kuchel, School of Molecular and Microbial Biosciences, Univ. of Sydney, NSW 2006, Australia. Tel.: +61-2-9351-3709; Fax: +61-2-9351-4726; E-mail: p.kuchel@mmb.usyd.edu.au.

0006-3495/02/07/161/11 $2.00

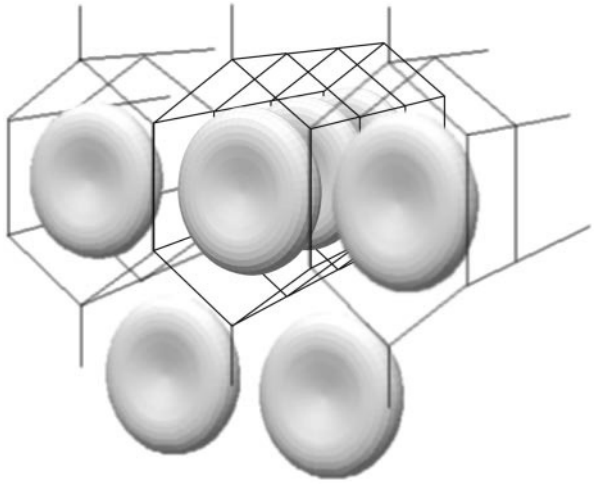

FIGURE 1 Hexagonal lattice of virtual cells. The figure illustrates the arrangement of cells (shown here as biconcave discs) used in the simulations of diffusion in the 3D infinite tessellation. The latter was effectively generated by the application of periodic boundary conditions to a unit cell.

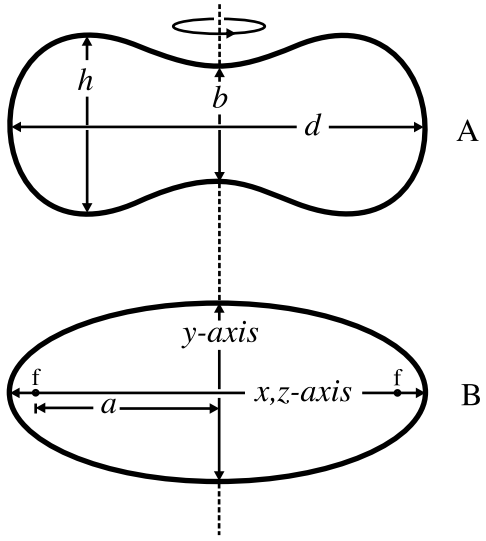

FIGURE 2 Cell geometry. (*A*) Two-dimensional representation of a biconcave disc whose shape and dimensions are defined by the parameters *b*, *d*, and *h* approximating those of a human red blood cell. (*B*) Two-dimensional representation of an oblate spheroid whose shape is defined by the parameters *a* (the distance from the foci, f, to the center of the oblate spheroid) and η (not shown) whose values are calculated as a function of the *x*-, *y*-, and *z*-semi-axis values using Eq. 2 and Eq. 3. Rotation around the axis indicated by the dotted line generates the 3D cell shapes used in the simulations.

NMR experiment (Kuchel et al., 1997; Torres et al., 1998) and produce an array of signal intensities corresponding to the respective field gradient strengths specified for a simulated experiment.

The programs use a Monte Carlo technique to simulate diffusion in a three-dimensional (3D) hexagonal lattice of "virtual" cells (see Fig. 1) as described previously (Lennon and Kuchel, 1994a,b; Torres et al., 1998). The uniform arrangement of virtual cells in a hexagonal lattice, having an order parameter of unity, is justified on the basis that real RBC align in the magnetic field, and that it was the intention to design a canonical pure system to form the basis of the interpretation of experimental *q*-space data (see Discussion).

Simulations were performed for ensembles of up to 10^8 noninteracting point molecules on a 64 processor SGI Origin 2400 supercomputer (APAC National Facility, Australian National Univ., Canberra, Australia). The intrinsic ensemble nature of the calculations allowed ensembles to be split into smaller "packets" of ~200,000 point-molecule trajectories, which could be distributed across multiple processors. In this way the parallel capability of the supercomputer was used. When the full complement of trajectories was completed, the results were summed and averaged.

The simulations were of diffusion in a 3D hexagonal lattice of cells having either biconcave disc (Fig. 2 *A*) or oblate spheroid (Fig. 2 *B*) geometry. The analysis was expedited by invoking a "unit cell," consisting of a regular hexagonal prism containing a cell, centered on the Cartesian origin, and applying periodic boundary conditions, thereby simulating an infinite tessellation. (In all simulations and experiments discussed in this report, a Cartesian coordinate system was used such that the *z* axis was aligned with the static magnetic field, $\mathbf{B}_0$, of the NMR spectrometer.) A random number generator and a random binary-digit generator were used to determine a random starting position for the trajectory of each point molecule (Regan and Kuchel, 2000). The same random number and random binary-digit generators were used to test for membrane transition and to choose random jump directions, respectively.

The biconcave disc in Program I was represented by a degree-4 equation in Cartesian coordinates (Kuchel and Fackerell, 1999). The shape of the biconcave disc (Fig. 2 *A*) was defined by the three parameters: *b*, thickness in the dimpled region; *h*, maximum thickness; and *d*, main diameter, whose respective values of 1.0×10^{-6} m, 2.12×10^{-6} m, and 8.0×10^{-6} m were assigned to closely approach the shape of human RBC and to yield the known mean volume of human RBC of 8.6×10^{-17} m^3 (Dacie and Lewis, 1975). The points of intersection of point-molecule trajectories with the biconcave disc were calculated using a Newton–Raphson algorithm (Regan and Kuchel, 2000).

The oblate spheroid used in Program II is described by the function

$$\frac{x^2}{a^2\cosh^2\eta} + \frac{y^2}{a^2\cosh^2\eta} + \frac{z^2}{a^2\sinh^2\eta} = 1, \qquad (1)$$

where, *a* is the distance of the foci from the center of the oblate spheroid (Fig. 2 *B*), and the oblate spheroidal coordinate η is a constant (Moon and Spencer, 1988). The values of *a* and η were calculated, as functions of the specified values for the oblate spheroid semi-axes, using the formulae

$$\eta = \frac{\ln((1 + r)/(1 - r))}{2} \qquad r = \frac{x}{y}; \qquad (2)$$

$$a = y/\sinh\,\eta, \qquad (3)$$

where *x*, *y*, and *z* are the values of the oblate spheroid semi-axes (Fig. 2 *B*) for the body centered at the origin of a Cartesian coordinate system. The *x*, *y*, and *z* semi-axes were assigned values of 8.0×10^{-6} m, 2.0×10^{-6} m, and 8.0×10^{-6} m, respectively. These values were chosen to match the overall dimensions of the biconcave disc but yielded a smaller volume of 6.7×10^{-17} m^3.

Another characteristic of a virtual cell that is useful for interpreting PGSE NMR data is the mean barrier separation in the cell. This value was calculated for both cell types in the *x*, *z*, and *y* directions. The calculation was performed by assigning a random coordinate inside the cell and calculating the length of the chord, in the relevant direction (*x*, *z*, or *y*), that intersected this point. This process was repeated for 10^7 random coordinates and the average chord length calculated. The mean barrier separation in the *x*, *z*, and *y* directions for the biconcave disc and the oblate spheroid were 5.8×10^{-6} m, 5.8×10^{-6} m, and 1.8×10^{-6} m, and 6.0×10^{-6} m, 6.0×10^{-6} m, and 1.5×10^{-6} m, respectively.

For each cell type, the following simulations were performed: diffusant (water) confined by an impermeable membrane to the intracellular space; diffusant confined by an impermeable membrane to the extracellular space, and packing density or hematocrit (Ht, the volume fraction of the unit cell that is occupied by a cell) set to either 0.3, 0.4, or 0.5; and diffusant in both the intracellular and extracellular spaces and able to exchange through a semi-permeable membrane, with hematocrits (Ht) set to 0.3, 0.4, or 0.5.

Intracellular (D_{in}) and extracellular (D_{out}) diffusion coefficients were assigned values of 1.6×10^{-9} m^2s^{-1} and 8.0×10^{-10} m^2s^{-1}, respectively, in accordance with preliminary estimates we have obtained experimentally (using standard PGSE NMR methods) for water in human RBC suspensions. The length of a jump, s, was calculated using the Einstein diffusion equation (Tanford, 1961),

$$\langle s^2 \rangle = 2D_{in/out}t, \quad (4)$$

where D is the diffusion coefficient in the relevant compartment (i.e., D_{in} or D_{out}), and t is the duration of a single jump (as determined from the assignment of other simulation parameters). For simulations in which the membrane was semi-permeable, the permeability (P_d) was assigned a value of 6.1×10^{-5} m s^{-1} as has been determined experimentally for human RBC (Benga et al., 1990). For simulations in which the membrane was required to be impermeable, P_d was set to zero.

We have previously demonstrated that the probability of transition across the membrane (tp) when the membrane is intersected by a point-molecule trajectory, in the context of the simulations described here, is related to s (jump length) and P_d by (Regan and Kuchel, 2000)

$$tp = P_d s/D_{in/out}. \quad (5)$$

The value of tp, therefore, depends on whether transition across the membrane is from the intra- or extracellular space.

The parameter values for the simulations were chosen to be identical to those used for the PGSE NMR experiments on RBC suspensions described in the Results. The PGSE NMR parameters for all simulations were as follows: field-gradient pulse duration, $\delta = 2$ ms; time interval separating field-gradient pulses, $\Delta = 20$ ms; the magnitude of the field-gradient, g, was sequentially incremented in 96 steps from 0.0 to 9.9 T m^{-1}; proton magnetogyric ratio, $\gamma = 2.675 \times 10^8$ radian T^{-1}. The phase shifts accumulated during the total diffusion time ($\delta + \Delta$) for all point-molecule trajectories were summed and averaged, and the signal intensity calculated for each value of **g**.

It has been shown that magnetic susceptibility differences between the interior and exterior of oxygenated or carbonmonoxygenated RBC in a suspension are negligible (Endre et al., 1984). Hence the model did not incorporate differences in PGSE signal intensity that might ordinarily be expected to occur in a system that is heterogeneous in magnetic susceptibility and hence magnetic field.

PGSE NMR experiments

PGSE NMR diffusion experiments were conducted on RBC suspensions having HT values of 0.2, 0.3, 0.4, 0.5, and 0.6. The general methods (pulse sequences, etc.) used for conducting these experiments and for preparing RBC suspensions were as described previously (Kuchel et al., 1997; Torres et al., 1998, 1999).

The experiments were conducted at 298 K on a Bruker AMX400 spectrometer (Karlsruhe, Germany) with an Oxford Instruments 9.4 T vertical wide-bore magnet (Oxford, UK), using a Bruker 10 T m^{-1}, z-axis gradient-diffusion probe. Identical pulse-sequence parameters were used for all experiments as follows: field-gradient pulse duration, $\delta = 2$ ms; time interval separating gradient pulses, $\Delta = 20$ ms; 32 transients per spectrum. The magnitude of the field-gradient was incremented from 0.001 to 9.9 T m^{-1} in 32 equal steps. (Unless the first spectrum [corresponding to the smallest field gradient] was acquired with a small nonzero gradient, its phase was substantially different from the rest in the series; therefore a value close to zero (0.01 T m^{-1}) was used.) The gradients were calibrated using the known diffusion coefficient of water in an isotropic and unbounded region (Mills, 1973).

The signal intensity was measured as the integral of the water resonance after automatic phase and baseline correction. Signal intensities were normalized with respect to that of the first spectrum before q-space analysis (see Data Analysis).

Data Analysis

q-Space analysis

q-Space plots were generated using both Origin (Microcal Software, Northampton, MA) and MATLAB (The Mathworks, Natick, MA) from simulated or experimental PGSE NMR data by plotting the normalized signal intensities as a function of the magnitude of **q**. A semi-logarithmic scale (logarithmic in the ordinate) was used to improve visualization of the features (maxima and minima) of the plots. Further enhancement was achieved by either applying a cubic spline to the data, or fitting a polynomial and interpolating points to increase their number from 96 to 1000. Simulated data invariably contained negative values at the extreme minimal intensities (see Discussion for an explanation of this phenomenon); these points could not be plotted on a logarithmic scale and thus resulted in gaps in the plots (see Figs. 3–6).

A combination of methods was used to determine, as precisely as possible, the positions of maxima and minima in q-space plots (the reciprocals of which correspond to mean dynamic displacements). Maxima and minima were determined, to a first approximation, by reading the values directly from the plot using the tools available in the respective plotting programs (Origin or MATLAB). This was not possible when data points were missing in semi-logarithmic plots due to negative signal intensities. This problem was obviated by replotting the absolute values of the signal intensities, again on a semi-logarithmic scale, so that regions containing negative values appeared as inverted peaks with q values that could be readily determined. Maximum and minimum values were then more closely pinpointed by aligning the putative values with maxima and minima in the plots of the first and second derivatives of the data (generated in MATLAB). In most cases, it was possible to determine accurately the positions of at least the first two maxima and minima (see Error Analysis). This method can be applied in the analysis of q-space data for diffusion along any axis but was carried out here for diffusion in the z direction only.

Diffusion tensor calculations

A program was written in MATLAB to calculate the terms of the diffusion tensor from PGSE NMR data (either real or simulated) according to the method of Kuchel et al. (2000). The program takes the normalized signal intensities and their corresponding gradient values (in each of the x, y, z, xy, xz, yz, and xyz directions) as inputs. Linear regression calculates initial estimates of the terms of the diffusion tensor, which are then used to calculate the final values and confidence intervals by nonlinear regression. In all cases, five signal intensities were included in the analysis (the q-space plot is approximately a single exponential over this range of gradient strengths), starting at the second value (i.e., points 2–6; the first point was eliminated because it corresponded to $g = 0$ and resulted in "divide by zero"). The diagonal terms of the resulting diffusion tensor provided estimates of the apparent diffusion coefficients (D_{app}) in the x, y, and z directions. Diffusion tensor calculations were only performed for simulated data because the experimental data were limited to diffusion in the z direction only.

Fourier transform analysis

The Fourier transform of q-space data is, in most cases, approximately Gaussian (see Discussion) and thus yields an approximation of the trans-

lational displacement probability (Cory and Garroway, 1990). The width-at-half-height, $\Delta w_{1/2}$, of the peak in the Fourier transform plot can therefore be related to the effective root mean square displacement (RMSD), σ, by (Bailey, 1995)

$$\sigma = \frac{\Delta w_{1/2}}{2[2 \ln 2]^{1/2}}. \quad (6)$$

Plotting the Fourier transform, and calculation of the width-at-half-height, was achieved by means of a program written in MATLAB. The program displays a plot of the transformed data, that have been zero-filled where necessary to ensure that the number of data points is a power of two, and allows the height of the peak to be read directly from the plot. This step improves the efficiency of the fast Fourier transform algorithm. The width-at-half-height is calculated using a cubic interpolation function that returns the value of the abscissa at half the height measured in the previous step. This value is then doubled (since only positive displacements are plotted) to yield the effective RMSD.

Error analysis

Both linear and nonlinear regression analyses were conducted in Origin and MATLAB. Error analysis of q-space plots, as it affects the estimation of critical values of q and their uncertainty, is influenced by two factors: the intrinsic signal-to-noise of the NMR spectra, and the resolution in q that is determined by the interval between q values, that are under experimental control. This matter has been discussed previously (Torres et al., 1999) and elaborated upon recently (Benga et al., 2000). It is important to note that, under the experimental conditions used in the present work, the uncertainty in the estimates was dominated by the resolution in q; in other words, the constant differences in consecutive q values that were specified in each experiment determined the spatial resolution of the imaging method.

RESULTS

General

In this study, we conducted simulations of diffusion in lattices of virtual cells having either biconcave disc or oblate spheroidal geometry. Simulations were conducted under two conditions: water confined to the intra- and extracellular spaces in the absence of exchange, and water exchanging between the intra- and extracellular regions at a rate that was determined by $P_d = 6.1 \times 10^{-5}$ m s^{-1}. In all cases, except where water was confined to the intracellular region, simulations were conducted at Ht values of 0.3, 0.4, and 0.5. In addition, a series of PGSE NMR experiments were conducted on real RBC suspensions at Ht values of 0.2, 0.3, 0.4, 0.5, and 0.6, at 298 K. To facilitate comparisons with real data sets, the simulation parameters were chosen to be identical to those used in the real experiments.

Simulations: exchange off

Intracellular diffusion

The q-space plots for simulation of diffusion of water inside biconcave discs and oblate spheroids (no exchange across the membrane) are shown in Fig. 3. Signal intensities at given values of q were initially higher for the oblate spheroid but were lower for the second and subsequent peaks. The apparent diffusion coefficients (D_{app}), estimated from diffusion tensor analysis (see Table 1), were smaller for the oblate spheroid than for the biconcave disc in each of the respective x, y, and z directions. For each cell type individually, however, the apparent diffusion coefficients measured in the x and z directions were identical within the stated error range. A similar trend was observed for the RMSD calculated from the Fourier transform of the q-space data (see Table 2): RMSD values were smaller for the oblate spheroid than for the biconcave disc in their respective directions and, in each case, had virtually identical values in the x, z, and xz directions as anticipated. The smallest values of D_{app} and RMSD for both cell types were observed in the y direction. The critical values in q space are given in Table 3. Although the relevant values in this case are the minima, which we have previously shown can be related to mean cell dimensions (Benga et al., 2000; Torres et al., 1998), both maxima and minima are given for completeness. The q value of the first minimum was smaller for the biconcave disc than for the oblate spheroid, corresponding to a larger dynamic displacement (q^{-1}), but there was no significant difference in the positions of the second minimum.

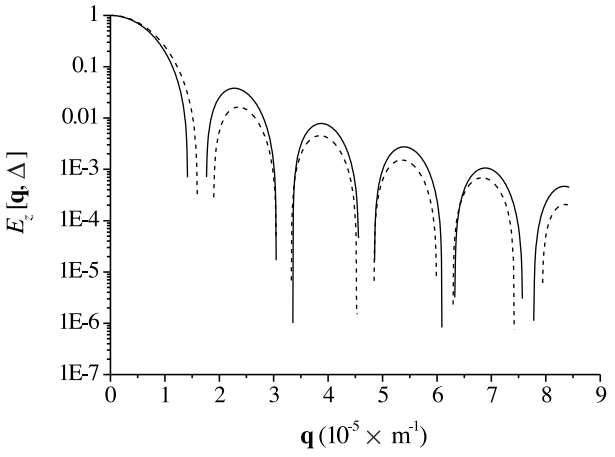

FIGURE 3 Simulation of diffusion in the intracellular spaces. q-Space plots derived from simulations of water diffusion inside biconcave discs (*solid line*) and oblate spheroids (*dashed line*). Point molecules were confined to the intracellular space by starting all trajectories inside the cell and setting P_d to zero.

Extracellular diffusion

Figure 4 shows the q-space plots for diffusion of water in the extracellular region of suspensions of oblate spheroids (A) and biconcave discs (B) at Ht values of 0.3, 0.4, and 0.5. The figure illustrates two important features: a shift in the positions of the peaks to higher q values as Ht was increased and, with respect to the first peak, higher signal intensities as Ht was increased. Table 3 confirms the shift to higher q values (smaller dynamic displacements) as Ht is increased;

TABLE 1 Apparent diffusion coefficients of water, from simulated data, as a function of packing density of the cells and the direction of the applied magnetic field gradient

		Biconcave Disc D_{app} ($10^9 \times m^2\ s^{-1}$)			Oblate Spheroid D_{app} ($10^9 \times m^2\ s^{-1}$)		
Exchange*	Ht	D_{xx}	D_{yy}	D_{zz}	D_{xx}	D_{yy}	D_{zz}
On	0.3	1.81 ± 0.14	0.95 ± 0.07	1.81 ± 0.14	1.82 ± 0.12	0.84 ± 0.05	1.82 ± 0.12
	0.4	1.52 ± 0.12	0.73 ± 0.06	1.52 ± 0.12	1.56 ± 0.10	0.62 ± 0.05	1.56 ± 0.10
	0.5	1.28 ± 0.10	0.56 ± 0.05	1.28 ± 0.10	1.33 ± 0.08	0.46 ± 0.04	1.33 ± 0.08
Off_{extra}	0.3	2.73 ± 0.07	1.43 ± 0.03	2.74 ± 0.07	2.70 ± 0.06	1.22 ± 0.02	2.70 ± 0.06
	0.4	2.61 ± 0.06	1.26 ± 0.03	2.62 ± 0.06	2.63 ± 0.06	1.03 ± 0.02	2.64 ± 0.06
	0.5	2.53 ± 0.06	1.15 ± 0.02	2.54 ± 0.06	2.58 ± 0.06	0.88 ± 0.02	2.59 ± 0.06
Off_{intra}		0.18 ± 0.0009	0.0047 ± 0.0007	0.18 ± 0.0009	0.16 ± 0.0006	0.0026 ± 0.0005	0.16 ± 0.0006

Values were obtained using diffusion tensor analysis.

*In this and subsequent tables: exchange "off" refers to simulations in which the diffusant was confined to either the intra- or extracellular region as indicated by the subscript; exchange "on" refers to simulations where exchange was allowed to occur between the two regions; and "endogenous" (Tables 2 and 3 only) refers to real PGSE NMR experiments on RBC suspensions in which exchange was occurring naturally at a rate determined by $P_d = 6.1 \times 10^{-5}$ m s^{-1}. Note also that a Ht value is not relevant for simulations where diffusion was confined to the intracellular space, where it is independent of the packing density, hence no value is given. The errors associated with the estimates of D correspond to ± one standard deviation.

in this case, the relevant values are the positions of the maxima because we have shown these to be related to the mean spacing of cells in the suspension (Torres et al., 1999). At all three Ht values, the corresponding dynamic displacements (q^{-1}) were higher for the biconcave discs than for the oblate spheroids. The apparent diffusion coefficients (Table 1) decreased as Ht was increased and, although of similar magnitude for both cell types in the x and z directions (when associated errors were considered), they were larger for the biconcave discs in the y direction. RMSD values (Table 2) were similarly decreased with increasing Ht and were of generally larger magnitude for the biconcave discs.

Simulations: exchange on

The results of simulations in which water was diffusing in both the intra- and extracellular regions and exchanging across the membrane are shown in Fig. 5. Signal intensities at given q values became larger as Ht was increased, and the pore-hopping shoulder (in the region of $q = 0.75 \times 10^5$ m^{-1}) shifted to higher q values and became less pronounced.

q-Space plots for the two cell types when the diffusion was measured in the x, y, and z directions are compared in Fig. 6. Points to note are: 1) the overall increase in signal

TABLE 2 Root mean square displacements estimated from Fourier transform analysis of *q*-space plots from simulated and experimental data

			RMSD ($10^6 \times$ m)						
System	Exchange	Ht	x	y	z	xy	xz	yz	xyz
Oblate Spheroid									
	On	0.3	13.74	6.04	13.54	11.18	13.63	11.11	11.92
		0.4	12.34	4.44	12.16	9.72	11.27	9.66	10.63
		0.5	11.13	3.63	11.74	8.56	11.08	8.50	9.43
	Off_{extra}	0.3	18.65	4.41	18.69	15.57	18.70	15.61	16.61
		0.4	18.33	3.18	18.46	15.09	18.47	15.14	16.32
		0.5	18.17	0.76	18.14	14.73	18.24	14.73	16.01
	Off_{intra}		4.95	0.39	4.95	3.49	4.95	3.49	4.06
Biconcave Disc									
	On	0.3	13.37	4.89	13.49	11.00	13.42	10.97	11.82
		0.4	11.89	3.59	11.78	9.40	11.89	9.42	10.30
		0.5	10.54	1.20	10.17	8.22	10.55	8.17	9.01
	Off_{extra}	0.3	18.56	5.21	18.98	16.08	18.98	16.08	17.01
		0.4	17.87	3.22	18.34	15.56	18.54	15.51	16.50
		0.5	17.12	1.73	17.98	15.14	18.13	15.10	16.17
	Off_{intra}		5.25	0.70	5.25	3.73	5.25	3.72	4.30
RBC Suspension									
	Endogenous	0.2			14.51				
		0.3			13.40				
		0.4			12.43				
		0.5			11.13				
		0.6			9.67				

TABLE 3 *q*-Values and dynamic displacements measured in the *z* direction from *q*-space plots of simulated and experimental data*

			q-values (q; $10^{-5} \times m^{-1}$) and corresponding dynamic displacements (q^{-1}; $10^6 \times m$)							
			$q_{1,min}$		$q_{2,min}$		$q_{1,max}$		$q_{2,max}$	
System	Exchange	Ht	q	q^{-1}	q	q^{-1}	q	q^{-1}	q	q^{-1}
Oblate Spheroid										
	On	0.3	1.75	5.70	3.12	3.21	0.72	13.95	2.20	4.54
		0.4	1.77	5.65	3.24	3.09	0.75	13.31	2.31	4.34
		0.5	1.51	6.62	3.22	3.10	0.79	12.72	2.39	4.18
	Off_{extra}	0.3	0.96	10.43	2.20	4.54	1.32	7.57	2.57	3.90
		0.4	1.01	9.90	2.31	4.34	1.39	7.19	2.70	3.70
		0.5	1.05	9.57	2.43	4.12	1.43	7.02	2.82	3.54
	Off_{intra}		1.75	5.70	3.19	3.14	2.36	4.24	3.86	2.59
Biconcave Disc										
	On	0.3	1.62	6.19	3.34	2.99	0.68	14.66	2.10	4.76
		0.4	1.62	6.19	3.17	3.15	0.73	13.62	2.19	4.58
		0.5	1.46	6.85	3.17	3.15	0.77	13.01	2.27	4.40
	Off_{extra}	0.3	0.89	11.24	2.05	4.89	1.27	7.88	2.44	4.09
		0.4	0.96	10.4	2.19	4.58	1.34	7.47	2.57	3.90
		0.5	1.01	9.90	2.27	4.40	1.39	7.19	2.69	3.72
	Off_{intra}		1.58	6.33	3.18	3.14	2.27	4.40	3.88	2.58
RBC Suspension										
	Endogenous	0.2	1.88	5.31			0.96	10.40	2.29	4.37
		0.3	1.87	5.36			0.97	10.35	2.25	4.44
		0.4	1.83	5.47			0.97	10.29	2.21	4.53
		0.5	1.83	5.47			0.97	10.29	2.24	4.47
		0.6	1.82	5.50			0.95	10.56	2.24	4.47

*Because q^{-1} was rounded to two decimal places from its original calculated value (i.e., not from the rounded value of q), two table entries may have the same value of q and slightly different values of q^{-1}.

attenuation at given q values for the oblate spheroid relative to the biconcave disc; 2) a shift in the positions of coherence maxima to higher q values for the oblate spheroid; 3) a much lesser degree of signal attenuation, for a given q value, in the y direction than in the x and z directions for both cell types; and 4) the appearance of some additional critical points (Fig. 6 *A*, $q = 2.3 \times 10^5$ m^{-1} and 4.2×10^5 m^{-1}, and relative to Fig. 6 *C*) in the plots for the x direction, which were otherwise very similar to those for the z direction for both cell types.

The apparent diffusion coefficients estimated from the diffusion tensor analysis (Table 1) decreased with increasing Ht. In the x and z directions, D_{app} values were virtually identical for both cell types but were larger for the biconcave disc in the y direction. In contrast, RMSD values (Table 2) were higher for the oblate spheroid than for the biconcave disc at equivalent Ht values. However, the same trend of decreasing RMSD with increasing Ht was observed for both cell types. Although no clear trend was evident in the positions of the first two diffraction minima ($q_{1,min}$ and $q_{2,min}$) for either cell type, the positions of the pore-hopping shoulder ($q_{1,max}$) corresponded to smaller dynamic displacements as Ht was increased and the respective values were smaller for the biconcave disc than for the oblate spheroid.

PGSE NMR experiments

The q-space plots of the PGSE NMR data obtained from real RBC suspensions are shown in Fig. 7. These plots illustrate two very clear results: signal intensities decreased at a given q value with decreasing Ht, and the point of inflection discernible at $q = \sim 1.0 \times 10^5$ m^{-1} was more pronounced at lower Ht.

Note that the high-power diffusion probe used in these experiments only allowed for the application of the magnetic field gradient coaxially with the static field (i.e., in the z direction). This limitation precluded the calculation of a diffusion tensor because this requires the gradient to be applied in at least six directions. In addition, the gradient values used in the experiment were restricted to a range over which it was possible to obtain sufficient signal-to-noise. Although it was possible to observe higher-order coherences with higher gradients, estimation of displacements from the data became increasingly error prone.

Fourier transform analysis of these data (Table 2) clearly showed that as Ht was increased the values of RMSD decreased. The relationship between RMSD and Ht was remarkably linear as evidenced by linear regression onto the data, which yielded the expression RMSD = $(1.70 \pm 0.02) \times 10^7 - ((1.20 \pm 0.05) \times$ Ht), with a correlation

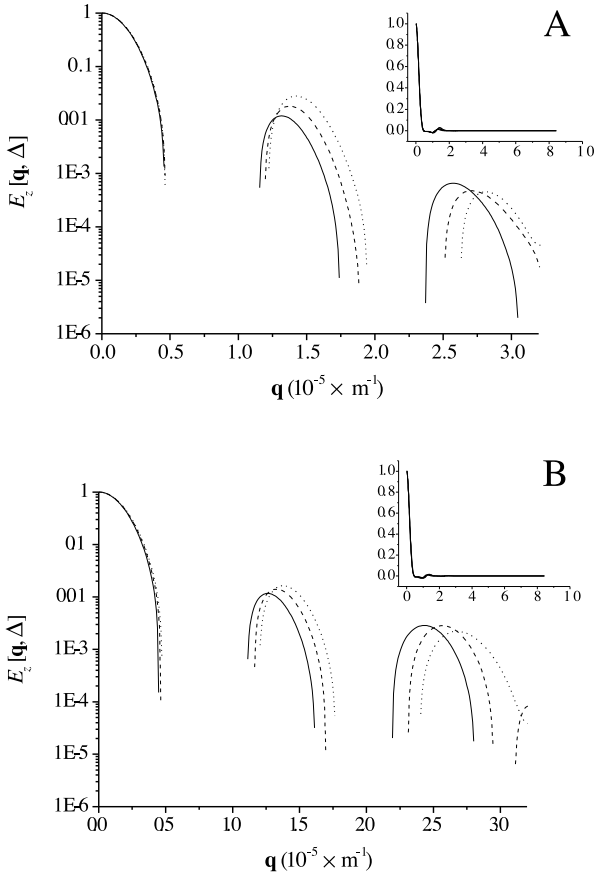

FIGURE 4 Simulation of diffusion in the extracellular spaces. q-Space plots derived from simulations of water diffusion in the extracellular region measured in the z direction in (*A*) a lattice of oblate spheroids, and (*B*) a lattice of biconcave discs. The main graphs were plotted on a semi-logarithmic scale and were discontinuous in the regions containing (minutely) negative signal intensities. The insets were plotted on normal axes to show that the data were continuous over the entire range of **q**. The simulations were performed using a range of packing densities: Ht = 0.3 (*solid line*); Ht = 0.4 (*dashed line*); and Ht = 0.5 (*dotted line*). Molecules studied were confined to the extracellular space by starting all trajectories outside the cell and setting P_d to zero.

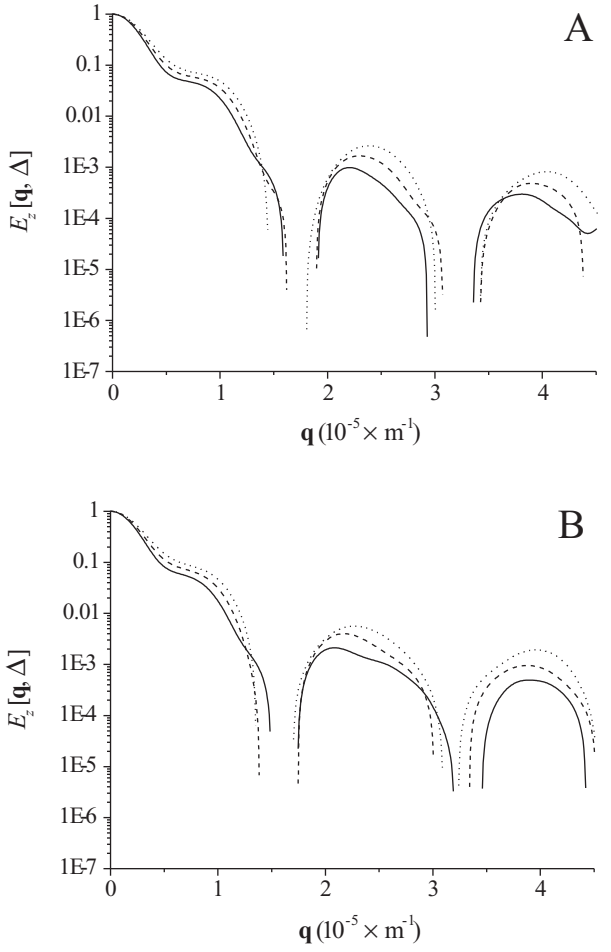

FIGURE 5 Simulations of diffusion in both the intra- and extracellular regions in (*A*) a lattice of oblate spheroids, and (*B*) a lattice of biconcave discs. The q-space plots were derived using measurements of diffusion of water in the z direction, and the exchange across the membrane occurred at a rate that was determined by $P_d = 6.1 \times 10^{-5}$ m s^{-1}. The simulations were performed using a range of packing densities: Ht = 0.3 (*solid line*); Ht = 0.4 (*dashed line*); and Ht = 0.5 (*dotted line*).

coefficient of −0.99. However, dynamic displacements calculated from q-space data were difficult to determine using the analytical methods that have been developed so far, and no clear trends were apparent in the values estimated. Although the dynamic displacements corresponding to $q_{1,min}$, $q_{1,max}$, and $q_{2,max}$ were smaller than the corresponding values for the simulated data from biconcave discs and oblate spheroids, they were of comparable magnitude.

DISCUSSION

Simulations: exchange off

We have considered two cases of simulation in which exchange across the membrane was prevented by setting P_d to zero. The first case was where the diffusant (water) inside the cells alone was studied. The second case was where the diffusant in the extracellular region alone was studied. In the latter case, simulations were conducted at three Ht values, 0.3, 0.4, and 0.5.

Intracellular diffusion

Figure 3 illustrates that overall signal attenuation (for diffusion in the z direction) for the oblate spheroid was greater than for the biconcave disc despite having a smaller volume, identical main-axis dimensions, and larger mean barrier separation in this direction. This seemingly counterintuitive result can be explained in terms of the shape of the biconcave disc. It has inward protrusions at its center that have a closest approach of 1×10^{-6} m constituting a kind of bottleneck restriction to diffusion in the z direction. In the initial part of the q-space curve in Fig. 3, the signal intensity

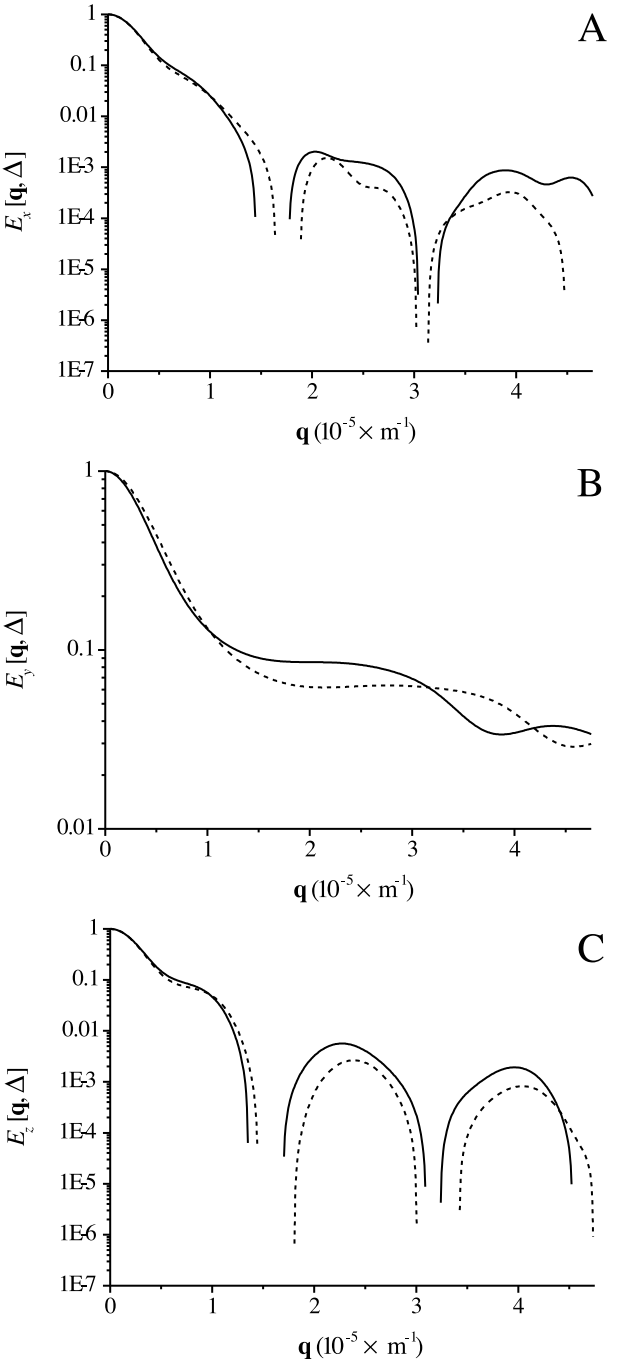

FIGURE 6 Simulated q-space plots derived for water diffusion in suspensions of biconcave discs (*solid lines*) and oblate spheroids (*dashed lines*) measured in (*A*) the x direction, (*B*) the y direction, and (*C*) the z direction. The transmembrane exchange rate was determined by $P_d = 6.1 \times 10^5$ m s^{-1} and Ht was 0.5.

is higher for the oblate spheroid than for the biconcave disc; and it was this region of the curve that was used for diffusion tensor analysis. Consequently, the apparent diffusion coefficients calculated using this method (Table 1) appear to be inconsistent with the result just described, i.e.,

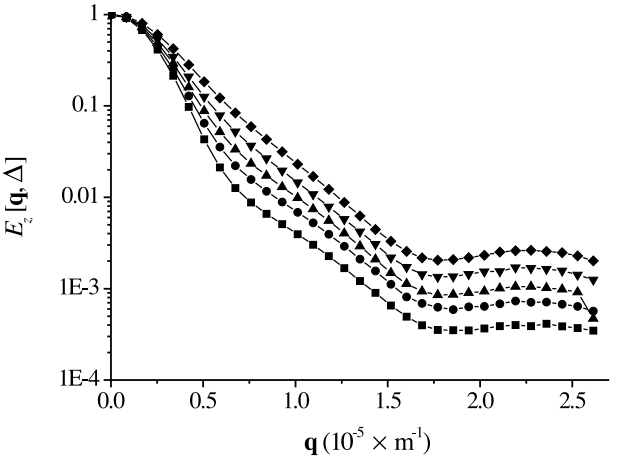

FIGURE 7 Experimental q-space data from PGSE NMR experiments on RBC suspensions having Ht = 0.2 (*square*), 0.3 (*circle*), 0.4 (*triangle*), 0.5 (*inverted triangle*), and 0.6 (*diamond*). Features of particular interest are $q_{1,max}$ at $\sim 1 \times 10^5$ m^{-1} and $q_{1,min}$ at $\sim 1.75 \times 10^5$ m^{-1}.

the D_{app} values are smaller for the oblate spheroid than for the biconcave disc. For both cell types individually, these values were the same in the x and z directions, reflecting the fact that, in these directions, their dimensions are identical, and much lower in the y direction, which is the direction in which diffusion was most restricted. The smaller volume occupied by the oblate spheroid is reflected in the smaller RMSD values (Table 2) with identical values recorded for both cell types individually in the x, z, and xz directions, in which the dimensions were identical. The critical q values (Table 3) in this case are the minima ($q_{1,min}$ and $q_{2,min}$) which are related to cell dimensions. Although both cell types had identical dimensions in the z direction, and the positions of $q_{2,min}$ did indeed yield identical estimates of the dynamic displacements, the positions of $q_{1,min}$ were not identical and suggest a smaller effective mean dimension in the z direction for the oblate spheroid than for the biconcave disc. These and the RMSD values reflect the fact that, although both cell types had identical main dimensions in x and z directions, their shapes and hence their mean dimensions along these axes were not identical.

Extracellular diffusion

The greater degree of signal attenuation that accompanied a decrease in Ht (see Fig. 4) was consistent with the notion that, as the compartment bounding the diffusant becomes less confining, the apparent diffusion coefficient will become larger, resulting in a more rapid attenuation of the signal in the PGSE NMR experiment. Table 1 shows that, as Ht was lowered, the apparent diffusion coefficient in the x, y, and z directions (as estimated by diffusion tensor analysis), increased for both cell types. Predictably, a decrease in Ht, and hence an increase in D_{app}, gave rise to an increase

in the RMSD calculated from the Fourier transform of the corresponding q-space plots (Table 2). Slightly higher values of RMSD estimated for the biconcave disc in most directions highlights the fact that, at equivalent Ht values, there was a greater volume available to the diffusant in this suspension because the volume of each biconcave disc was greater. The few exceptions to this observation, revealed by careful comparison of the data, are attributed to differences in the cell shapes that, in turn, give rise to differently shaped pores in the extracellular region.

The observation that, for both biconcave discs and oblate spheroids, the signal intensity at a given q value in the second peak of the q-space plot increased as Ht was decreased (i.e., opposite to the anticipated result that is observed for the first peak) is explained as follows. The position of the second peak results from a second-order effect i.e., displacement of molecules between next-nearest neighboring pores. At lower Ht values, the RMSD is larger so there is a higher probability of displacement occurring into these pores (in the observation time of the experiment) than for a higher Ht. The number of spins giving rise to this signal at low Ht will consequently be larger than the number at a higher Ht. Thus, the resulting signal intensity will be relatively higher (i.e., relative to that at higher Ht) than for diffusion between the first coordination layer of cells.

The data in Tables 1 and 2 indicate that, for the oblate spheroids, the effect of changing Ht is more dramatic for diffusion measured in the y direction than in other directions (particularly those not containing a y component). The y direction is orthogonal to the disc planes of the virtual cell and is therefore the most confining for the diffusant. Therefore, it is anticipated that relaxing the impediment to diffusion in this direction (by reducing Ht) will have a dramatic effect on the estimated apparent diffusion coefficient and thus the RMSD. This effect is less dramatic for the biconcave disc, and the reason for this can be understood as follows: The dimpled regions of the biconcave disc result in diffusion orthogonal to the disc planes being, on average, less restricted than for oblate spheroids. Hence, the effect on the RMSD of increasing the distance between the discs is less dramatic with biconcave discs.

We noted above that the critical values in the q-space plots, in this case, the pore-hopping maxima $q_{1,\max}$ and $q_{2,\max}$, are related to the spacing of the major extracellular pores in the array. As Ht was increased, the q values of these critical points would be expected to become larger (and their reciprocal values, the dynamic displacements, become smaller), and this was indeed the case (Table 3). A larger q value corresponds to a smaller dynamic displacement, and, as Ht was increased (i.e., the hexagonal prism containing the unit cell was made smaller), the distance between the centers of adjacent pores became smaller. The hexagonal prism enclosing the biconcave disc was larger than that for the oblate spheroid because the volume of the cell was larger. This explains the slightly larger dynamic displacements observed for the biconcave disc. For the oblate spheroid, the scaling factors relating the position of $q_{1,\max}^{-1}$ and $q_{2,\max}^{-1}$ to the cell diameter were: 1.06 and 2.05 for Ht = 0.3; 1.11 and 2.16 for Ht = 0.4; and 1.14 and 2.26 for Ht = 0.5. For the biconcave disc, the scaling factors were: 1.02 and 1.96 for Ht = 0.3; 1.07 and 2.05 for Ht = 0.4; and 1.11 and 2.15 for Ht = 0.5. For the latter of these relationships, i.e., for the biconcave disc at Ht = 0.5, we previously reported scaling factors of 1.063 and 2.146; these are in close agreement with those values obtained here.

Simulations: exchange on

The simulations of diffusion involved identical systems to those described in the section above, but they were conducted with exchange occurring between the intra- and extracellular regions. Molecules were assigned initial coordinates either inside or outside the virtual cell in a random manner, with a distribution (inside or outside) that was determined by the Ht. One measure of the robustness, or reproducibility, of these simulations was that, at a given Ht, the final distribution of point molecules between the intra- and extracellular spaces did not change to a statistically significant extent from the initial distribution.

Relative to the simulations of diffusion in which exchange was absent, decreasing the Ht resulted in a greater degree of signal attenuation with increasing q value (Fig. 5). Again, this is attributable to the diffusant in the extracellular region being less restricted as the spacing between the cells was increased. This observation is reinforced by the estimates of the D_{app} and RMSD values, which, without exception, increased with decreasing Ht (Tables 1 and 2). It is also notable that the pore-hopping shoulder was more pronounced at lower Ht values as a result of the proportionally increased contribution to the signal from the extracellular water. The additional critical points observed in Fig. 6 *A* arise from the fundamentally different topological arrangement of pores and cells in a hexagonal array when projected in the x and z directions.

The data in Table 2 show that RMSD values were slightly smaller for the biconcave disc than for the oblate spheroid. This result is opposite from that obtained for either intra- or extracellular diffusion in the absence of exchange. Thus the estimate of the apparent diffusion coefficient (directly related to the RMSD) in a two-compartment system with exchange is a nonlinear weighted sum of the apparent values in each compartment.

PGSE NMR experiments

The simulations described above were conducted to improve our interpretation of data obtained from PGSE NMR experiments on real cellular systems. It was shown that the

biconcave disc simulations did indeed give rise to features that were seen in q-space plots from RBC suspensions.

However, as seen from (Fig. 7) and previous reports (Benga et al., 2000; Kuchel et al., 1997; Torres et al., 1998, 1999), the various features and critical points of the q-space plots were less pronounced than for the simulated canonical data. This is readily interpreted as being due to real RBC suspensions having a distribution of cell sizes and, to a lesser extent, shapes. In addition, the cells in a real suspension in the NMR spectrometer, although virtually completely aligned in the z direction, will not be so aligned in the x and y directions. Also, they move slightly during each NMR pulse sequence and therefore will be arranged in a continuously changing and random manner. The simulations were conducted on systems in which all cells were identical both in size and shape, and their orientations were exactly specified with their packing arrangement fixed and regular. Further work could entail building in random fluctuations in cell orientation and this would lead to a blurring of the features of q-space plots.

It is also clear from the experimental data (Fig. 7) that the extent of signal attenuation was increased at all values of q as Ht was decreased, as occurred with the simulated data. The pore-hopping shoulder was more pronounced at lower values of Ht, and this is attributed to the greater volume of water in the extracellular region resulting in its greater contribution to the overall water signal. However, had the Ht been further decreased, it is anticipated that, at some value, this feature would have become less pronounced and eventually disappeared altogether as the extracellular pores would have become ill-defined.

Also in Fig. 7, a decrease in Ht was accompanied by an increase in RMSD, reflecting the diminished restriction to diffusion in the extracellular region afforded by the lower volume occupied by the RBC. Once again, this result was observed in the simulations. The relationship between Ht and RMSD was very linear (see Results), thus suggesting a method for estimating the Ht of a sample simply by measuring the width-at-half-height of the Fourier transform of the q-space plot. The RMSD at Ht = 0.5 was considerably higher than that for the biconcave discs at the same Ht, and was closer to that for the oblate spheroids. The reason for the discrepancy lies in the values chosen for the intra- and extracellular diffusion coefficients for which only preliminary experimental values were used in the simulations.

The features of the q-space plots in Fig. 7 are not highly resolved, and, consequently, determination of the critical q-values was more difficult than for the simulated data. Nevertheless, the relationships between critical values and characteristics of the cells in the suspension at Ht = 0.5 are comparable with the simulated data at Ht = 0.5.

General points

It has been pointed out above that, in a real RBC suspension, the cells are not of identical size and are not motionless in a regular lattice. The models used in this study, in contrast, were based on an ideal and hence simplified system. The intention in the work was not merely to provide a simplification but rather to develop a canonical system that would reveal features that would be difficult to discern in a more realistic system due to the blurring effect of randomization of cell orientation.

The degree of signal attenuation in the PGSE NMR experiments on real RBC suspensions extended to greater than 10^3. Despite this high level of attenuation, we are able to ignore the contaminating signals from other cellular metabolites or components. The concentration of water protons in the cell is 70–80 M and close to 100 M in the extracellular fluid. The concentration of nonexchangeable glycyl protons from glutathione, the most abundant metabolite inside the cells, is just 4 mM, a factor of 10^5 lower than water. The hemoglobin concentration, although significantly higher, has a short T_2 relaxation time, so, in PGSE NMR experiments with an echo time of greater than 20 ms, the hemoglobin makes no significant contribution to the signal in the region of the water resonance (Kuchel and Chapman, 1991).

A complicating factor in the analysis of simulation data has been the appearance of negative signal values at the minima. The magnitude of these negative echoes was, on average, of the order of 10^{-5} of the initial signal intensity. Although methods have been developed to overcome this difficulty (see Materials and Methods), considerable thought was given to the origin of this phenomenon. At the much less than Avogadro's number of trajectories performed for any single simulation, there will always be an excess of displacements in the ensemble in either the positive or negative direction along any axis. Any excess, however small, will constitute a degree of apparent flow and will give rise to negative spin-echo signal intensities (Callaghan et al., 1999).

q-Space data from real or simulated cell suspensions is clearly not Gaussian, and, consequently, the propagator obtained from the Fourier transform of the data is also not Gaussian. However, fitting a Gaussian to a typical q-space data set yielded a width-at-half-height of $(2.27 \pm 0.01) \times 10^4$ m with a correlation coefficient of 0.99. Therefore, on the basis that the propagator is approximately Gaussian, we contend that the width-at-half-height of the Fourier transform of q-space data is related to the effective RMSD (see Eq. 6).

CONCLUSIONS

We used random walk simulations of diffusion to study the relationship between the features of NMR q-space data and the shapes of the cells in the sample. Different cell geometries gave rise to differences in features in the q-space plots, so this finding will be useful in detecting pathological changes in cells and in the identification of cell types

(Torres et al., 1998). We have pointed out the differences that exist between the simulated and real-cell suspensions. The ideality of the simulated systems has, in fact, allowed us to identify features in q-space plots that appear with lower resolution in such plots from real RBC suspensions. Thus, we could assign these features of q-space plots to particular modes of diffusion in an ideal setting. Two methods for facilitating the analysis were described: first- and second-derivative analysis of q-space plots for the determination of q values of critical points in q-space plots, and Fourier transform analysis for calculating apparent RMSD values. The latter method provides a quick and simple means of determining the Ht of cell suspensions. Finally, we used diffusion tensor analysis to estimate the apparent diffusion coefficients and to show their dependence on direction of movement of the diffusant in a heterogeneous system, such as a suspension of cells with only one axis of symmetry.

The work was supported by grants from the Australian National Health and Medical Research Council and the Australian Research Council to P.W.K., and an Australian Postgraduate Award to D.G.R.

We thank Dr. Bob Chapman and Dr. Bill Bubb for assistance with the NMR spectroscopy, and Mr. Bill Lowe for technical assistance.

REFERENCES

Bailey, N. T. J. 1995. Statistical Methods in Biology. Cambridge University Press, Cambridge, UK.

Benga, G., P. W. Kuchel, B. E. Chapman, G. C. Cox, I. Ghiran, and C. H. Gallagher. 2000. Comparative cell shape and diffusional water permeability of red blood cells from Indian elephant (*Elephas maximus*) and Man (*Homo sapiens*). *Compar. Haematol. Int.* 10:1–8.

Benga, G., V. I. Pop, O. Popescu, and V. Borza. 1990. On measuring the diffusional water permeability of human red blood cells and ghosts by nuclear magnetic resonance. *J. Biochem. Biophys. Methods.* 21:87–102.

Callaghan, P. T., S. L. Codd, and J. D. Seymour. 1999. Spatial coherence phenomena arising from translational spin motion in gradient spin echo experiments. *Concepts Magn. Reson.* 11:181–202.

Callaghan, P. T., A. Coy, D. MacGowan, K. J. Packer, and F. O. Zelaya. 1991. Diffraction-like effects in NMR diffusion studies of fluids in porous solids. *Nature.* 351:467–469.

Cory, D. G., and A. N. Garroway. 1990. Measurement of translational displacement probabilities by NMR: an indicator of compartmentation. *Magn. Reson. Med.* 14:435–444.

Dacie, J. V., and S. M. Lewis. 1975. Practical Haematology. Churchill Livingstone, London.

Endre, Z. H., B. E. Chapman, and P. W. Kuchel. 1984. Cell volume dependence of ^{1}H spin-echo signals in human erythrocytes suspensions: the influence of in situ field gradients. *Biochim. Biophys. Acta.* 803: 137–144.

Higashi, T., A. Yamagishi, T. Takeuchi, N. Kawaguchi, S. Sagawa, S. Onishi, and M. Date. 1993. Orientation of erythrocytes in a strong static magnetic field. *Blood.* 82:1328–1334.

Kuchel, P. W., and B. E. Chapman. 1991. Translational diffusion of hemoglobin in human erythrocytes and hemolysates. *J. Magn. Reson.* 94:574–580.

Kuchel, P. W., A. Coy, and P. Stilbs. 1997. NMR "diffusion-diffraction" of water revealing alignment of erythrocytes in a magnetic field and their dimensions and membrane transport characteristics. *Magn. Reson. Med.* 37:637–643.

Kuchel, P. W., C. J. Durrant, B. E. Chapman, P. S. Jarrett, and D. G. Regan. 2000. Evidence of red cell alignment in the magnetic field of an NMR spectrometer based on the diffusion tensor of water. *J. Magn. Reson.* 145:291–301.

Kuchel, P. W., and E. D. Fackerell. 1999. Parametric-equation representation of biconcave erythrocytes. *Bull. Math. Biol.* 61:209–220.

Lennon, A. J., and P. W. Kuchel. 1994a. Enhancement of the "diffraction-like" effect in NMR diffusion experiments. *J. Magn. Reson. A.* 111: 208–211.

Lennon, A. J., and P. W. Kuchel. 1994b. Neural networks used to interpret pulsed-gradient restricted-diffusion data. *J. Magn. Reson. A.* 107: 229–235.

Mansfield, P., and P. K. Grannell. 1973. NMR 'diffraction' in solids? *J. Phys. C: Solid State Phys.* 6:L422–L426.

Mills, R. 1973. Self-diffusion in normal and heavy water in the range 1–45°. *J. Phys. Chem.* 77:685–688.

Moon, P., and D. E. Spencer. 1988. Field Theory Handbook. Including Coordinate Systems, Differential Equations and Their Solutions. Springer-Verlag, Berlin.

Regan, D. G., and P. W. Kuchel. 2000. Mean residence time of molecules diffusing in a cell bounded by a semi-permeable membrane: Monte Carlo simulations and an expression relating membrane transition probability to permeability. *Eur. Biophys. J.* 29:221–227.

Tanford, C. 1961. Physical Chemistry of Macromolecules. John Wiley and Sons, New York.

Torres, A. M., R. J. Michniewicz, B. E. Chapman, G. A. R. Young, and P. W. Kuchel. 1998. Characterisation of erythrocyte shapes and sizes by NMR diffusion-diffraction of water: correlations with electron micrographs. *Magn. Reson. Imaging.* 16:423–434.

Torres, A. M., A. T. Taurins, D. G. Regan, B. E. Chapman, and P. W. Kuchel. 1999. Assignment of coherence features in NMR q-space plots to particular diffusion modes in erythrocyte suspensions. *J. Magn. Reson.* 138:135–143.